Journal of Molecular Structure 1133 (2017) 226–235

Contents lists available at ScienceDirect

Journal of Molecular Structure

journal homepage: http://www.elsevier.com/locate/molstruc

Structural properties and FTIR-Raman spectra of the anti-hypertensive clonidine hydrochloride agent and their dimeric species

Elida Romano [a], Lilian Davies [b], Silvia Antonia Brandán [a, *]

[a] Cátedra de Química General, Instituto de Química Inorgánica, Facultad de Bioquímica, Química y Farmacia, Universidad Nacional de Tucumán, Ayacucho 471, 4000, San Miguel de Tucumán, Tucumán, Argentina
[b] Instituto de Investigaciones para la Industria Química (INIQUI, CONICET), Universidad Nacional de Salta, Av. Bolivia 5150, 4400, Salta, Argentina

ARTICLE INFO

Article history:
Received 16 September 2016
Received in revised form
30 November 2016
Accepted 2 December 2016
Available online 5 December 2016

Keywords:
Clonidine hydrochloride
Vibrational spectra
Molecular structure
Force field
DFT calculations

ABSTRACT

The structural and vibrational properties of the α-adrenergic agonist clonidine hydrochloride agent and their anionic and dimeric species were studied combining the experimental FT-IR and Raman spectra in solid phase with ab-initio calculations based on the density functional theory (DFT). All the calculations were performed by using the hybrid B3LYP with the 6-31G* and 6-311++G** basis sets. The structural properties for those species were studied employing the Natural Bond Orbital (NBO), Atoms in Molecules theory (AIM) and frontier orbitals calculations. The complete assignments of the FTIR and Raman spectra were performed combining the DFT calculations with the Pulay's Scaled Quantum Mechanics Force Field (SQMFF) methodology. Very good concordances between the theoretical and experimental spectra were found. In addition, the force constants for those three species were computed and compared with the values reported for similar antihypertensive agents. The ionic nature of the H→Cl bond and the high value of the *LP(1)N4 → LP*(1)H18* charge transfer could explain the high reactivity of clonidine hydrochloride in relation to other antihypertensive agent and the strong shifthing of the band assigned to the N–H stretching mode linked to the H–Cl bond toward lower wavenumbers.

1. Introduction

The heterocyclic compounds containing furan, phenyl and imidazoline rings in its structures can act as potent agonists and antagonists of imidazoline receptors [1–6] because the activity of the furan ring increase when the phenyl group is incorporate in the structure [3] and, for this reason, they are broadly used in the therapy hypertensive, for example clonidine hydrochloride [1,2,4,5]. The knowledge of the structures and vibrational properties of these antihypertensive agents are essential for their quick identifications, for the synthesis of new derivatives with pharmacologic properties improved and, to know and explain their behaviours and mode of action. In this sense, the imidazoline derivatives, such as the two antihypertensive agents, 2-(-2-benzofuranyl)-2-imidazoline and tolazoline hydrochloride whose structures and vibrational properties were recently reported by Contreras et al. [7,8] are of great chemical, biochemical and mainly pharmacological interest. In this work, we have studied the antihypertensive clonidine hydrochloride agent, whose chemical name is 2-[2,6-dichlorophenylamino]-2-imidazolidine hydrochloride. Remko et al. [4] have reported the theoretical structures, p*K*a, lipophilicity, solubility, absorption, and polar surface area for some centrally acting antihypertensive agents, including the geometries of various tautomers of clonidine. But, so far, the vibrational properties and the infrared and Raman spectra of clonidine hydrochloride even remain without to assign. The interpretation of the vibrational spectra is of particular relevance to identify these species in different systems and pharmaceutical products by using the vibrational spectroscopy. The aim of this work is to report the complete vibrational analysis of clonidine hydrochloride and their anionic and dimeric species combining the FTIR and FT-Raman spectra with DFT calculations and the Scaled Quantum Mechanic Force Field (SQMFF) methodology [9]. For these purposes, the structures of the clonidine hydrochloride and their anionic and dimeric species were optimized by using the 6-31G* and 6-311++G** basis sets, and later, their corresponding frequencies were calculated. In addition, the electronic and topological properties of the dichlorophenyl and imidazoline rings were evaluated by means of natural bond orbital (NBO) [10,11] and Atoms in

* Corresponding author.
E-mail address: sbrandan@fbqf.unt.edu.ar (S.A. Brandán).

http://dx.doi.org/10.1016/j.molstruc.2016.12.008
0022-2860/

Molecules (AIM) [12,13] calculations in order to know their structural properties. The reactions sites of these species with the α-adrenoceptors were analyzed by using the molecular electrostatic potential surfaces. The prediction of the reactivity of clonidine hydrochloride was performed using the frontier orbitals.

2. Experimental methods

A pure anhydrous Aldrich commercial sample of clonidine hydrochloride was used. The IR spectrum of the solid substance in KBr pellets (2 mg of solid sample in 200 mg of KBr) was recorded in the wavenumbers range from 4000 to 400 cm^{-1} with an FT-IR Perkin Elmer spectrophotometer, provided with a Globar source and DGTS detector. The Raman spectra of the compound in solid state was recorded between 4000 and 100 cm^{-1} with a Bruker RF100/S spectrometer equipped with a Nd:YAG laser (excitation line of 1064 nm, 800 mW of laser power) and a Ge detector cooled at liquid nitrogen temperature. The IR and Raman spectra were recorded with a resolution of 1 cm^{-1} and 200 scans.

3. Computational details

The initial structures of clonidine hydrochloride (H), the anionic form (A) and their dimer (D) were first modelled with the *GaussView* program [14] and later optimized in gas phase by using the hybrid B3LYP method [15,16] and the 6-31G* and 6-311++G** basis sets with the Gaussian 09 program [17]. All the optimizations have converged to real minima confirmed by means of their positive frequencies. The optimized structures of H, A and D together with the atom's numberings can be seen in Fig. 1 while Fig. 2 shows the structure dimeric D. The energy of the dimeric species was corrected for basis set superposition error (BSSE) by the standard Boys–Bernardi counterpoise method [18]. The topological analysis for those species was performed by using the Bader's theory [12] and the AIM2000 program [13] while the NBO calculations were carry out with the NBO 3.1 [11] program in order to compute the natural population atomic (NPA) charges, the bond order and the stabilization energy values. The SQMFF procedure [9] and the Molvib program [19] were employed to calculate the force fields of the three species using those two approximation levels. The natural internal coordinates for the species were defined according to those reported in the literature for other antihypertensive agents [7,8] and, for this reason, they were not presented here. Then, the complete assignments of the bands observed in the vibrational spectra were performed taking into account the potential energy distributions (PED) and the corresponding internal coordinates proposed. The predicted Raman spectra were corrected from scattering activities to relative Raman intensity, taking into account the excitation frequency used in the measurements, according to the equations reported by Polavarapu and Keresztury et al. [20,21] and using the RAINT program reported by Michalska [22]. In addition, the force constants for those species were calculated from the corresponding scaled force fields which later were compared with those calculated for the antihypertensive agents, 2-(-2-benzofuranyl)-2-imidazoline and tolazoline hydrochloride [7,8].

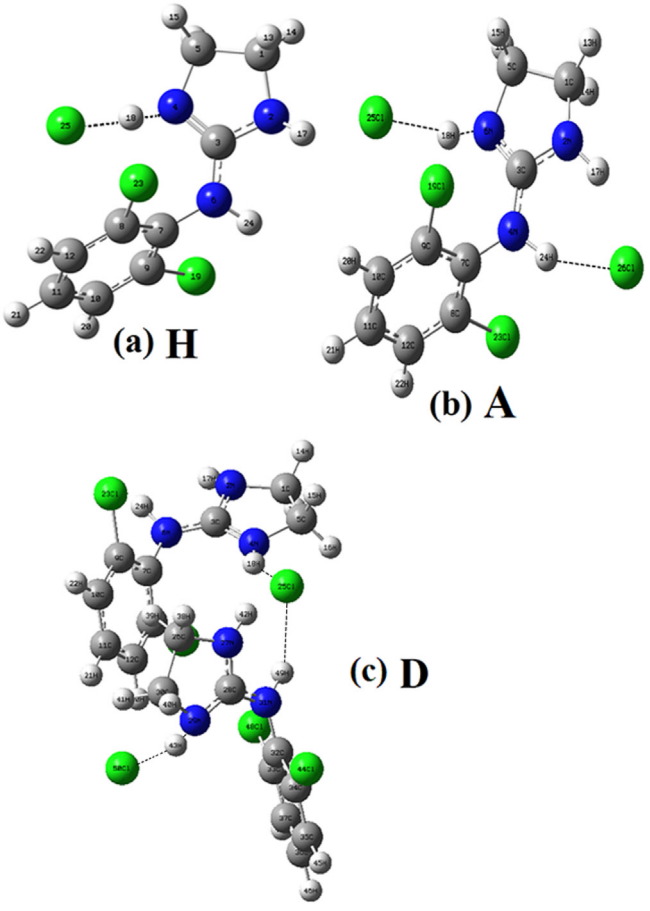

Fig. 1. Molecular structures of: (a) clonidine hydrochloride (H), (b) anionic form (A) and (c) the dimeric species (D) with the corresponding atoms numbering.

4. Results and discussion

4.1. Geometry optimization

A comparison of the total energies and the corresponding dipole moment values for H, A and D by using both methods can be seen in Table S1 (Supporting Material). Note that the presence of the dimeric species in the solid phase can in part be explained by their high stability even in the gas phase (−3788.1050 Hartrees using 6-31G* basis set considering correction by BSSE) because in this medium is most stable than the monomeric species ($2 \times -1893.8247 = -3787.6494$ Hartrees). Thus, the stability of D using both basis sets could also be explained due to their intermolecular H–Cl bonds. On the other hand, the high dipole moment values for the two neutral forms with both basis sets could in part explain their experimental stabilities, as was observed in different compounds [23–26]. The experimental 2-[2,6-dichlorophenylamino]-2-imidazolidine hydrochloride structure (named, clonidine hydrochloride), $C_9H_9N_3Cl_2 \cdot HCl$, belongs to monoclinic system with $M = 266.56$; $Z = 8$ and space group $C2/c$, was reported by Byre et al. [27] and compared in Table 1 with the corresponding theoretical ones for H and A. The theoretical anionic structure compared with the corresponding crystal structure of clonidine hydrochloride determined by X-ray diffraction showing the strong hydrogen bonds between the N–H bonds and Cl ions are observed in Fig. S1. The comparison between the theoretical values with the corresponding experimental ones was performed by means of the root mean of square deviation (RMSD) values. The bond N(2)–C(3) and C(3)–N(4) lengths belonging to the imidazoline ring are not chemically equivalent in the H and A species. Thus, the C(3)–N(4) distance shows a double bond character whereas the N(2)–C(3) distance evidence a partial double bond character. This result is very useful taking into account that in the agonist compounds, as clonidine hydrochloride, the positive charge is evenly distributed in the N–C–N region of the imidazole ring, as reported by Ghose and Dattagupta [28]. It is very important to clarify that the

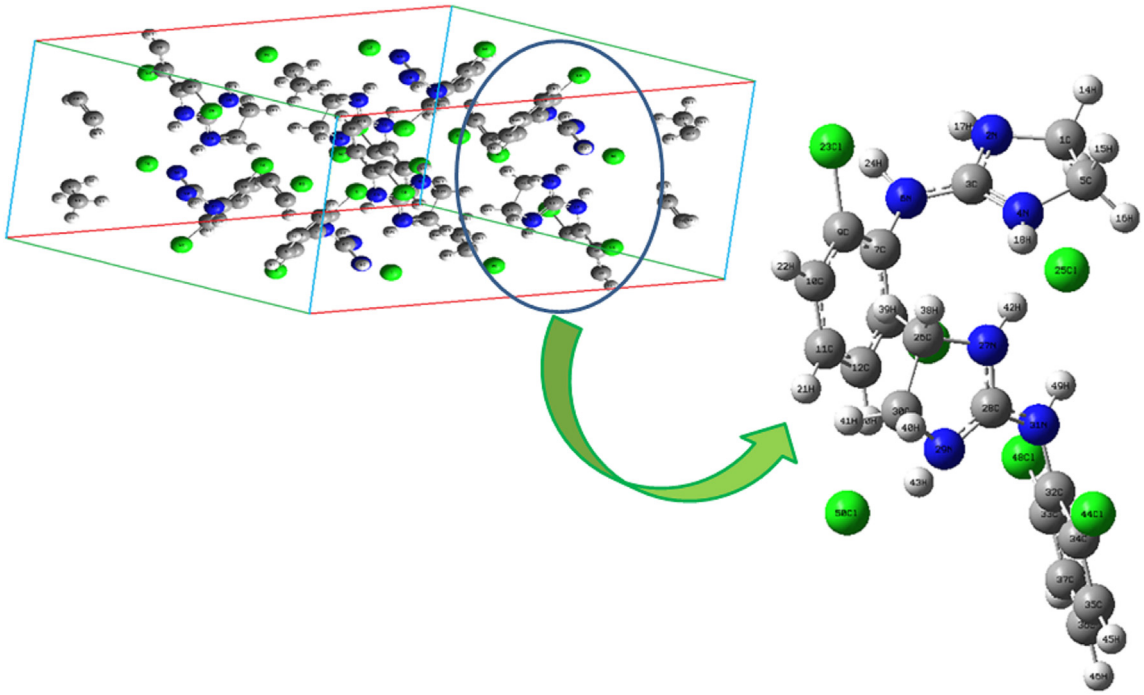

Fig. 2. Crystal packing of clonidine hydrochloride showing polymeric structure from Ref. [27] and the theoretical dimeric species (D).

B3LYP calculations in this species predicted the N2—H17 distance very different from that corresponding to N4—H18 which show values of 1.013 and 1.739 Å for H using the 6-31G* basis set, and for A values of 1.036 and 1.067 Å, respectively. Another very significant result for this species was found when we analyzed the Cl25—N4 distances because the calculations predicted values of 2.874 Å for H and 3.006 Å for A using the 6-31G* basis set and of 2.877 Å for H and 3.019 Å for A with the 6-311++G** basis set, which are different from the experimental ones (3.094 Å). Moreover, the bond C(3)-N(6) length in both species present a partial double bond character while the calculated bond C(3)-N(6)-C(7) angle value that connect to the two rings is closer to the experimental one. The lower RMSD values observed for H and A show a very good correlation in the two structures optimized with both basis sets, as observed in Table 1 and, the higher variations are observed in the dihedral angles, probably due to that the strong barrier of energy impedes the rotation of the two torsion angles at the same time, as observed for clonidine hydrochloride by X-ray diffraction by Byre et al. [27]. Note that the RMDS values favors to the anionic structure when the distance between the nitrogen atoms and the chlorine ions which form hydrogen bond are considered (see Table 1). These results give a reliable starting point for the determinations of the B3LYP/6-31G* and/or B3LYP/6-311++G** force fields and frequency calculations of these species.

4.2. Atomic charges, bond orders and electrostatic potentials studies

The influence of the nature of atoms or groups on the chemical and biological properties of an agonist drug is of interest to know and understanding the behaviours of these species in the receptor sites. Thus, the charge distribution is important to explain the mode of interaction of the agonist specie with the α-adrenergic receptor site, as reported by Ghose and Dattagupta [28]. Hence, we have studied the natural population atomic charges (NPA) [29,30] in order to evaluate the stability of clonidine hydrochloride due to the presence of three electronegative Cl atom in the structure. Thus, Table S2 shows the NPA charges and the bond orders, expressed as Wiberg's index for clonidine hydrochloride and their anionic species in gas phase at different theory levels. The most positive NPA values are observed on the C3 atoms belonging to the imidazole rings while the most negative values are observed on the Cl25 atom (in A and H) and on the Cl26 atom (only for A) linked to the N—H bond, as can be seen in Fig. 1. When the molecular electrostatic potential (MEP) surface mapped for H, A and D at B3LYP/6-31G* level are compared among them different reaction sites are observed, as shown in Figs. S2, S3 and S4, respectively. Fig. S2 shows a strong red colour on the Cl25 atom, in accordance with their higher NPA charge, suggesting this region as an electrophilic site, acceptor of H bonds while the strong blue colours are located on the N2—H17 and N6—H24 bonds indicating that these are nucleophilic sites, donor of H bonds. Analyzing the surface mapped of the D species (Fig. S4) we observed strong red colour on the Cl atoms, in agreement with the monomeric hydrochloride species while that in the ionic form (Fig. S3) can be only see a strong red colour on chloride anions, consistent with the most negative NPA charge values. Thus, the charges and MEP studies for the H and D species reveal clearly diverse reaction sites which implies different interaction with the α-adrenergic receptor sites. The bond orders, expressed as Wiberg's index for H and A are given in Table S2. The results revels that the bond order values are strongly dependent of the size of the basis sets, hence, the values are enlarged when increase the size of the basis set. The bond order values for the C8 and C9 atoms belong to the phenyl rings and linked to the Cl atoms have the highest values while the lowest values are calculated for the C1 and C5 atoms belonging to the imidazoline rings. Analyzing the bond order matrix by atoms we observed that the N4—H18 bond order presents a value of 0.477 in H and 0.5924 in A while the corresponding values to H18 → Cl25 is 0.350 for H and 0.1976 for A. These values show clearly the different nature and characteristics of both bonds that probably explain the biological properties of this compound.

Table 1
Comparison of calculated geometrical parameters for anionic and clonidine Hydrochloride forms with their corresponding experimental values.

B3LYP[a]					
		Hydrochloride		Anionic form	
Parameter	Exp.[b]	6-31G*	6-311++G**	6-31G*	6-311++G**
Bond lengths (Å)					
C(1)–N(2)	1.447	1.477	1.478	1.461	1.463
C(1)–C(5)	1.533	1.547	1.545	1.545	1.543
N(2)–C(3)	1.321	1.373	1.372	1.353	1.351
C(3)–N(4)	1.322	1.305	1.303	1.330	1.328
N(4)–C(5)	1.450	1.468	1.469	1.463	1.464
C(3)–N(6)	1.328	1.359	1.354	1.343	1.338
N(6)–C(7)	1.418	1.422	1.422	1.411	1.412
C(7)–C(8)	1.392	1.403	1.400	1.407	1.403
C(7)–C(9)	1.391	1.403	1.400	1.406	1.403
C(9)–C(10)	1.382	1.389	1.387	1.392	1.389
C(10)–C(11)	1.377	1.393	1.390	1.391	1.388
C(11)–C(12)	1.371	1.392	1.390	1.392	1.390
C(8)– C(12)	1.385	1.392	1.388	1.393	1.389
C(8)–Cl(23)	1.724	1.751	1.751	1.750	1.750
C(9)–Cl(19)	1.733	1.755	1.754	1.752	1.751
N(4)–Cl(25)	3.193	2.874	2.877	3.006	3.019
N(6)–Cl(26)	3.094			3.114	3.113
RMSD		**0.019**	**0.017**	**0.014**	**0.014**
RMSD[c]		**0.083**	**0.082**	**0.033**	**0.030**
Bond angles (°)					
C(1)–N(2)–C(3)	111.5	107.5	107.7	108.4	108.6
N(2)–C(3)–N(4)	111.8	113.6	113.4	112.4	112.1
N(2)–C(1)–C(5)	102.6	101.9	101.8	101.3	101.3
C(3)–N(4)–C(5)	110.6	109.4	109.7	108.9	109.1
C(1)–C(5)–N(4)	103.5	103.3	103.2	102.2	102.1
N(2)–C(3)–N(6)	123.1	119.8	120.2	120.4	120.6
C(3)–N(6)–C(7)	123.0	123.6	123.9	123.7	123.8
N(6)– C(3)–N(4)	125.2	126.5	126.4	127.3	127.2
N(6)–C(7)–C(8)	121.3	121.3	121.2	121.2	121.2
N(6)–C(7)–C(9)	121.4	120.6	120.7	121.6	121.5
C(8)–C(7)–C(9)	117.3	117.9	118.0	117.2	117.2
C(7)–C(9)–C(10)	121.5	121.6	121.5	121.7	121.7
C(9)–C(10)–C(11)	119.8	119.1	119.1	119.5	119.4
C(10)–C(11)–(12)	120.2	120.7	120.8	120.5	120.6
C(11)–C(12)–C(8)	119.8	119.5	119.4	119.3	119.3
C(12)–C(8)–C(7)	121.4	121.0	121.1	121.8	121.7
C(7)–C(9)–Cl(19)	120.0	119.1	119.2	119.8	119.7
C(10)–C(9)–Cl(19)	118.5	119.3	119.3	118.5	118.5
C(7)–C(8)–Cl(23)	119.9	120.1	120.0	119.5	119.4
C(12)–C(8)–Cl(23)	119.7	118.9	118.9	118.8	118.8
RMSD		**1.38**	**1.29**	**1.23**	**1.17**
Dihedral angles (°)					
N(2)–C(3)–N(6)–C(7)	178.1	177.8	178.7	174.4	173.9
N(4)–C(3)–N(6)–C(7)	0	−2.3	−1.1	−6.8	−7.2
C(3)–N(6)–C(7)–C(8)	−76.5	−73.4	−75.2	−74.0	−76.5
C(3)–N(6)–C(7)–C(9)	105.2	109.0	106.2	107.6	104.8
RMSD		**2.71**	**1.03**	**4.24**	**4.17**

[a] This work.
[b] Ref [23].
[c] RMSD considering the two N–Cl bonds.

4.3. NBO studies

The stabilities of H and A were also evaluated by using NBO calculations [11,12]. Then, for these species at the same levels of theory and in accordance with this methodology the second order perturbation energies that involve the most important delocalization were calculated and the results are given in Table S3 and S4. Note that, in total, there are eight delocalization energies for H of which four are the $\Delta ET_{\sigma\rightarrow\sigma^*}$, $\Delta ET_{\pi\rightarrow\pi^*}$, $\Delta ET_{LP\rightarrow\pi^*}$ and $\Delta ET_{\pi^*\rightarrow\pi^*}$ charge transfers while the other ones are those from the π, σ, π^* and *LP* orbitals to the *LP*H18* orbital, as observed in Table S3, which contributes to the high stability of this species. On the other hand, we observed that the stabilization energy values are strongly dependent of the size of the basis set because H present high ΔET_{Total} stabilization energy values with both basis sets, these are, 5036.19 kJ/mol using the 6-31G* basis set and 5446.69 kJ/mol when the 6-311++G** basis set. This NBO study for H has revealed that the $\Delta ET_{\pi\rightarrow\pi^*}$, $\Delta ET_{LP\rightarrow\pi^*}$ and $\Delta ET_{\pi^*\rightarrow\pi^*}$ charge transfers are the most important contributions to the stabilization energies mainly due to the phenyl ring, being that latter, the most important. These studies support the high stability of H due to the higher values observed in the *LP(1)N4 → LP*(1) H18* charge transfers with both levels of calculations. In relation to the anionic species, we observed four *LP(1)Cl → σ*(1)N–H* charge transfers with lower energy total values in relation to H form that clearly support the presence of the hydrogen bonds, as can be seen in Table S4 and as will also see in the AIM results.

4.4. AIM analysis

The Bader's theory is very interesting to investigate and characterize the type and nature of the inter- and intra-molecular interactions in the molecules, especially when these species present α-adrenergic agonist activity, as clonidine hydrochloride [13]. Thus, the localization of the bond critical points (BCPs) and ring critical points (RCPs) in the charge electron density, $\rho(r)$ and the *Laplacian* values, $\nabla^2\rho(r)$ for the two structures H and D were computed using the AIM2000 program [14]. These topological properties for the phenyl and imidazoline rings in the RCPs are given in Table S5 while the parameters corresponding to the BCPs and new RCPs are presented in Table S6. The exhaustive analysis shows clearly that the properties of the phenyl rings in both structures are practically the same, as expected, because in those structures the rings do not change while, the properties of the imidazoline rings are higher and slightly different among them for H, A and D species. Furthermore it is observed that the $\rho(r)$ and $\nabla^2\rho(r)$ values for the phenyl are lower than those corresponding to the imidazole ring, which clearly shows the different nature of both rings. This analysis it is necessary in H to determine the nature of the N4–H18 and H18 → Cl25 bonds found in the study by the Wiberg indexes. Thus, we observed that for the N4–H18 bond the $\lambda 1/\lambda 3 > 1$ and $\nabla^2\rho(r) < 0$ values with high values of $\rho(r)$ and $\nabla^2\rho(r)$ which implies that the interaction is typical of covalent bonds (called shared interaction) while for the H18→Cl25 bond the $\lambda 1/\lambda 3 < 1$ and $\nabla^2\rho(r) > 0$ indicated that the interaction is typical of ionic, highly polar covalent and hydrogen bonds as well as of the van-der-Waals intermolecular interactions (called closed-shell interaction). Obviously, for D, a similar result it is observed, as can be seen in Table S5. These studies show that the N4–H18 bond is covalent while the H18 → Cl25 bond has ionic character. Here, for the anionic species three H bonds are observed in agreement with the NBO analysis where the H_{17}–Cl_{26} interaction present two contributions to the stabilization energy, as shown Table S4.

4.5. Vibrational analysis

The structures of clonidine hydrochloride and their dimer have C_1 symmetries, where H has 69 vibration normal modes, D present 144 while A has 72 vibration normal modes. All the vibration modes of these species have activity in both IR and Raman spectra. The recorded infrared spectrum for H in solid phase can be seen in Fig. 3 and their corresponding Raman spectrum in Fig. 4. In both figures the experimental spectra were compared with the corresponding theoretical of the species predicted at the B3LYP/6-31G* level of theory. Both experimental spectra show the presence of

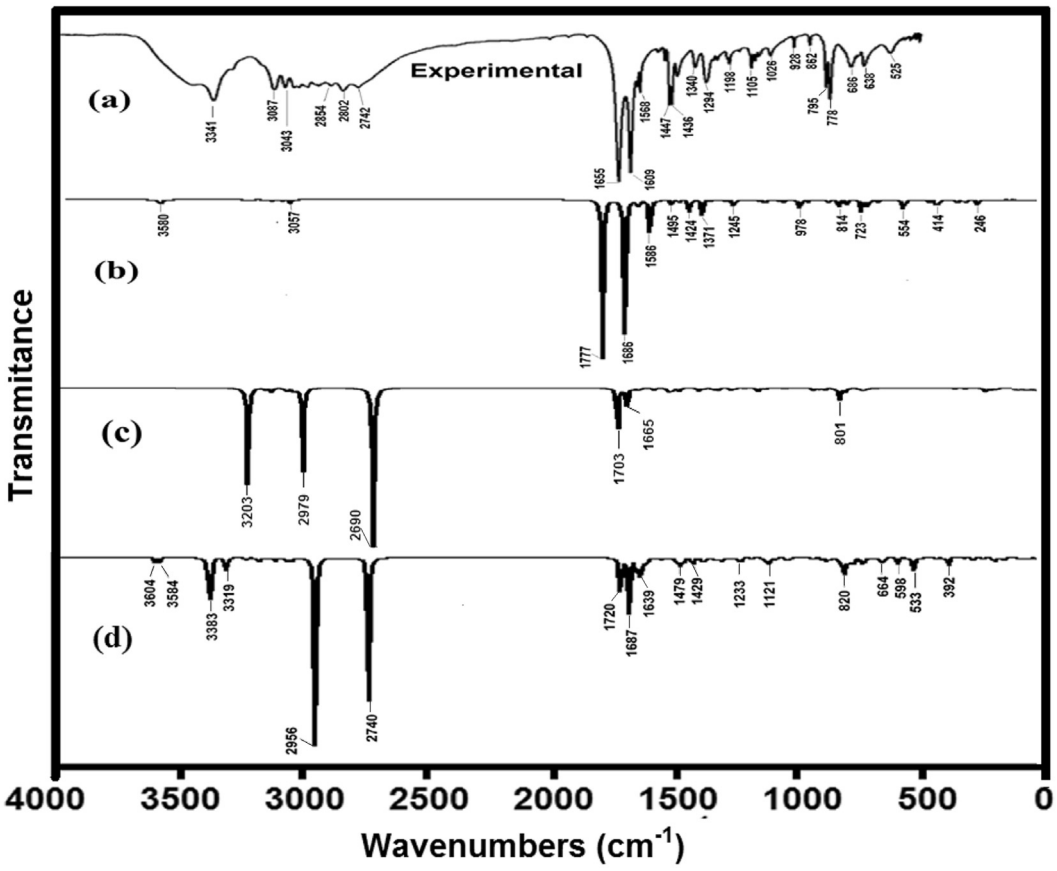

Fig. 3. Comparison between the experimental infrared spectra of clonidine hydrochloride in the solid phase (a) with the corresponding theoretical for the monomer (b), anionic form (c) and dimeric species (d) by using 6-31G* basis set.

bands attributed to these species. Table 2 shows the observed and calculated frequencies together with the assignments for those species studied. The complete assignments of experimental bands to the normal modes of vibration were performed taking into account the PED contributions by using the B3LYP/6-31G* method, the corresponding symmetry coordinates and the assignments of related molecules [7,8,22,24–28]. The scale factors used were those defined for the B3LYP/6-31G* method [10]. The assignment of the vibrational normal modes and the PED contributions based on the 6-31G* basis set for H and A are shown in Tables S7 and S8, respectively. To perform the assignments for these two forms from the resulting SQM only the PED contributions ≥10% were considered while that for D some contributions <10% were also considered due to that the vibration modes are strongly mixed. The SQM force fields for these species can be obtained at request. The assignments of some groups are discussed below.

4.5.1. Band assignments

4.5.1.1. NH modes. The bands between 3427 and 3341 cm^{-1} observed in both spectra of the solid are assigned to the N–H stretching modes, as observed in Table 2, except for the N–H bonds involved in Hydrogen bonds with the chlorine atom, which are 2859–2584 cm^{-1}. It is necessary to clarify that in the neutral monomer this mode corresponding to the N4–H18 bond is predicted at 1711 cm^{-1} (Table 2) because in the calculations the crystalline packing is not considered. The characteristic of the N4–H18 and H18→C25 bonds (supported by NBO and AIM studies) justify the notable shifting of this stretching mode. The in-plane deformations modes or bending modes are associated to the bands in the 1436-1340 cm^{-1} region, while the out-the plane deformations are associated to the shoulder at 618 cm^{-1} in the IR and to the intense band in the Raman spectrum at 505 cm^{-1} and a shoulder at 437 cm^{-1}, in agreement with similar compounds [7,8,29].

4.5.1.2. CN modes. The IR and Raman bands with different intensities observed at 1655 cm^{-1}, 1246 cm^{-1} and in Raman at 1014 cm^{-1} are assigned to the C–N stretching modes of the three species, as indicated in Table 2. Here, the weak Raman band at 1127 cm^{-1} is clearly assigned to the CN stretching modes of D, whereas the strong band at 443 cm^{-1} is assigned to the CNC deformation corresponding to the dimer while for H and A species this mode are predicted at smaller wavenumbers (63 and 111 cm^{-1}, respectively).

4.5.1.3. CH modes. The group of bands between 3087 and 3043 cm^{-1} in the IR spectrum and between 3093 and 3050 cm^{-1} region in the Raman spectrum are assigned to the C–H stretching modes, as observed in Table 2. As predicted by the calculations, the corresponding in-plane deformations modes are easily assigned to the IR bands at 1447 (1446 Ra), 1395 (Ra), 1198 and 1155 cm^{-1} (1157 Ra) while the bands at 973, 928 (929 Ra), 898 (Ra), 877 (Ra) and 778 cm^{-1} (778 Ra) are assigned to the corresponding out-the plane deformations for all the species. The very weak band at 260 cm^{-1} and other very strong at 220 cm^{-1} in the Raman spectrum can be easily assigned to the stretching modes related to the C–H–Cl modes corresponding to the monomer and dimer, respectively. This mode in the anionic species is assigned to the Raman band at 126 cm^{-1}.

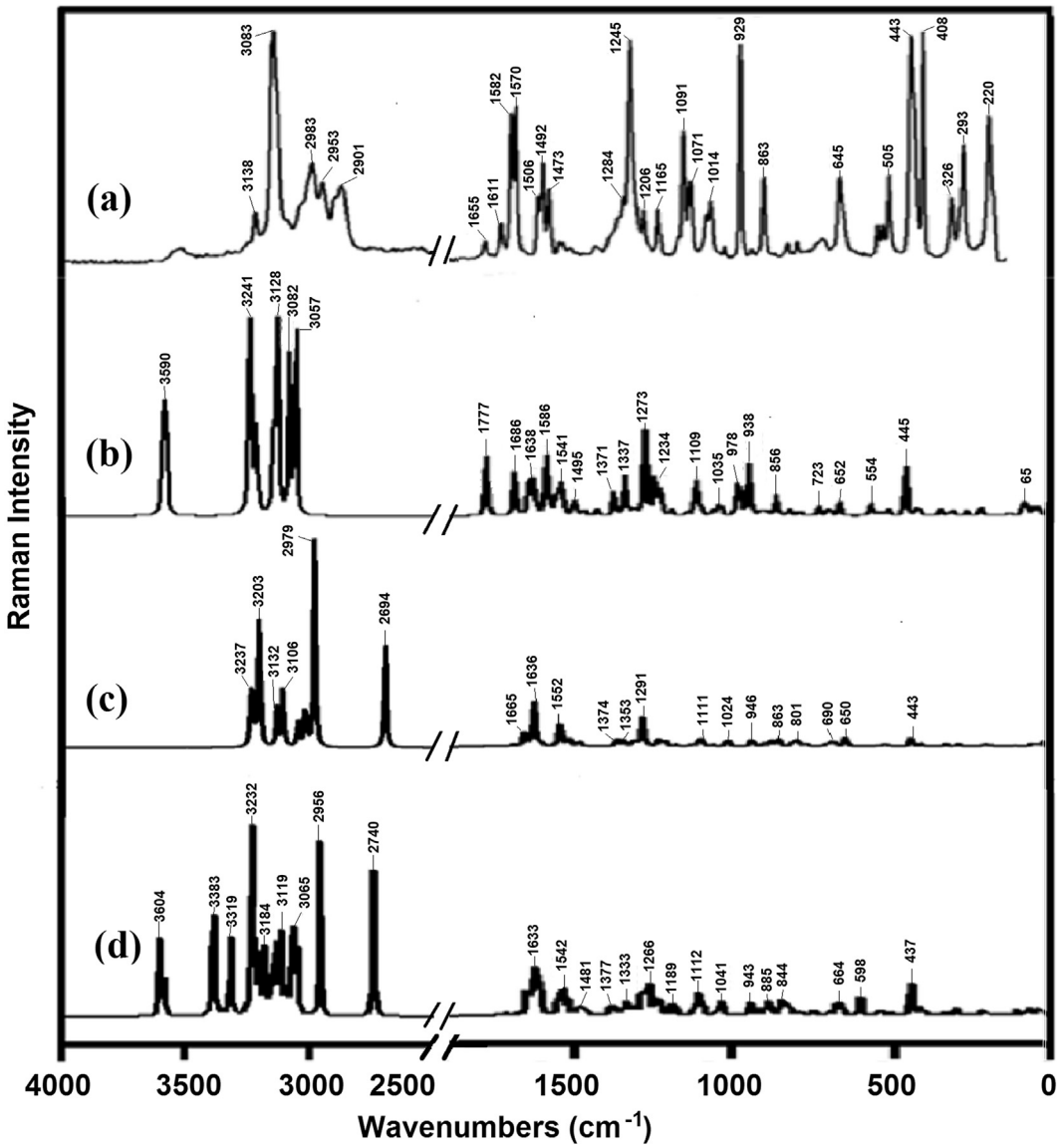

Fig. 4. Comparison between the experimental Raman spectra of clonidine hydrochloride in the solid phase (a) with the corresponding theoretical for the monomer (b), anionic form (c) and their dimeric species (d) by using 6-31G* basis set.

4.5.1.4. CH_2 modes. In all the studied species, the asymmetric and symmetric stretching modes are assigned between 3007 and 2906 cm^{-1}. In this compound, the asymmetric stretching modes are calculated at higher wavenumbers than the symmetric modes and, for this, the asymmetric modes can be assigned to the bands in IR and Raman spectra at 3007 and 2986 cm^{-1}, while the symmetric modes are assigned to the IR and Raman bands of medium intensity at 2960, 2950, 2920 and 2906 cm^{-1}, as can be seen in Table 2. The shoulder at 3135 cm^{-1} in IR and 3138 cm^{-1} medium intensity bands in Raman are assigned to asymmetric CH_2 stretching modes of D. The IR bands at 1493, 1485 and 1466 cm^{-1} are clearly assigned to the scissoring modes in agreement with similar compounds containing the CH_2 group [7,8,22,24–27] while, as predict the calculation, the medium IR bands at 1340 and 1294 cm^{-1} are easily assigned to the wagging modes. The expected rocking modes are assigned to the weak IR band at 1206 cm^{-1} and the Raman band at 1194 cm^{-1} [7,8,22,24–27]. The twisting modes are associated with the weak band and a shoulder in IR at 1026 and 812 cm^{-1} respectively, and the medium and weak Raman bands at 1028 and 987 cm^{-1} respectively.

4.5.1.5. Skeletal modes. The C=C stretching modes of phenyl ring was assigned to the bands at 1581, 1568, 1264 and 1075 cm^{-1}. The C–C stretching mode of imidazole ring does not appear in the IR spectrum, but a weak signal in Raman is observed in accordance to the related compounds [7,8,22,24–28]. The C–Cl stretching modes were assigned to the IR bands at 421 and 402 cm^{-1}. The corresponding in-plane deformation modes (bendings) appear in Raman as a shoulder at 303 cm^{-1} and a very weak band at 186 cm^{-1}. However, the corresponding out-of-plane deformation modes appear at 525 and 518 cm^{-1} in IR, as predicted by the calculations. Two weak bands in the IR spectrum at 1091 and 686 cm^{-1} are assigned to in-plane deformation modes of the phenyl ring (bendings). There are two signals that appear in the IR spectrum at 1111 cm^{-1} as a shoulder and a band of medium intensity at 1105 cm^{-1} that are assigned to in-plane deformation of the phenyl rings in the dimer. While for the imidazole ring these bands appear at 862 and 686 cm^{-1} in the IR, and in the Raman spectrum at

Table 2
Observed and calculated wavenumbers (cm^{-1}) and assignment for all forms of clonidine hydrochloride.

Experimental[a]		Hydrochloride[a]		Anionic Form[a]		Dimer[a]	
IR	Raman	SQM[b]	Assignment[a]	SQM[b]	Assignment[a]	SQM[b]	Assignment[a]
						3455	ν(N2–H17)
		3442	ν (N2–H17)			3436	ν(N6–H24)
3427 m, br	3422 vw	3432	ν (N6–H24)				
	3411 vw					3243	ν(N27–H42)
3341 s	3346 w, br					3182	ν(N31–H49)
3135 sh	3138 m			3103	ν(C10–H20)	3138	ν_{as} CH_2 (C1)
3087 s	3093 sh	3106	ν(C12–H22)	3093	ν(C12–H22)		
3087 s	3083 vs	3103	ν(C10–H20)	3071	ν (N2–H17)	3103	ν(C12–H20)
3043 m	3050 m	3081	ν(C11–H21)	3066	ν(C11–H21)	3053	ν(C11–H21)
3007 m	3005 sh	3011	ν_{as} CH_2 (C5)	3002	ν_{as} CH_2 (C5)	3026	$\nu_{as}CH_2$ (C5)
2986 m	2983 s	2998	ν_{as} CH_2 (C1)	2978	ν_{as} CH_2 (C1)	2990	$\nu_{as}CH_2$ (C26)
2960 sh		2955	ν_s CH_2 (C5)			2968	ν_s CH_2 (C5)
2950 m	2953 m	2930	ν_s CH_2 (C1)			2945	ν_s CH_2 (C30)
2920 sh	2919 m			2921	ν_s CH_2 (C5)	2938	ν_s CH_2 (C1)
2906 m	2901 m			2892	ν_s CH_2 (C1)	2923	ν_s CH_2 (C26)
2872 sh				2859	ν (N6–H24)	2836	ν (N6–H18)
2854 m	2822 vw					2836	ν (N4 –H18)
2802 m	2811 vw					2740	ν(N29–H43)
2742 m	2792 vw	1711	ν (N4–H18)	2584	ν (N4–H18)	2628	ν (N29–H43)
1655 vs	1655 m			1637	ν (C3–N6)	1657	ν (C3–N4); ν (C3–N6)
1655 vs	1655 m	1624	ν(C3–N4)	1604	ν (C3–N2)	1618	ν (C28–N31) ν (C28–N27)
1609 s	1611 m					1595	ν (C28–N29)
1581 m	1582 s	1583	ν(C8–C12)	1581	ν(C8–C12)	1578	ν (C33–C37)
1568 m	1570 s	1573	ν(C11–C12)			1574	ν (C3–N2)
	1542 sh			1563	ν(C11–C12)	1567	ν (C8–C12)
1506 w	1506 m	1519	ν (C3–N6)				
1493 w	1492 m	1487	δCH_2 (C1)	1487	δCH_2 (C1)	1488	δCH_2 (C1)
1485 w	1473 m	1473	δCH_2 (C5)	1482	ρ (N6–H24)	1474	δCH_2 (C5)
1466 w		1448	ν(C7–C8)	1462	δCH_2 (C5)	1443	ν (C32–C34)
1447 s	1446 m	1446	ν(C7–C9)	1444	β(C10–H20); ν(C7–C9)	1432	β (C12–H20)
1436 s	1436 w			1434	ν(C9–C10)	1429	β (C37–H47)
1414 m	1416 w, br					1413	β (N2–H17)
	1395 w	1406	β(C10–H20)	1399	β(N4–H18)	1380	β (N29–H43)
1385 sh	1380 w	1368	β(N4–H18)			1377	β (N4–H18)
1340 m	1342 w	1321	*wg* CH_2(C5)	1329	*wg* CH_2 (C5)	1346	*wg* CH_2 (C30)
1294 m	1293 sh	1295	*wg* CH_2(C1)	1304	β(N2–H17)	1300	*wg* CH_2 (C1)
	1278 sh	1285	ν(C9–C10)	1274	*wg* CH_2 (C1)	1285	ν (C7–C9)
1264 w	1264 m	1251	ρ (N6–H24)	1260	ν(C7–C8)	1263	ν(C32–C33)
1246 w	1245 s	1235	ν(C7–N6)	1247	ν(C7–N6)	1243	ν(C32–N31)
1206 w	1206 m	1212	β(N2–H17)	1219	ρ CH_2 (C5)	1206	ρCH_2 (C26) ρCH_2 (C30)
1198 w		1198	β(C12–H22)	1196	β(C12–H22)	1198	β(C35–H45) ν(C34–C35)
	1194 sh	1195	ρ CH_2 (C5) ρ CH_2 (C1)	1190	ρ CH_2 (C1)	1192	ν (C9–C10)
	1165 m						
1155 vw	1157 sh	1156	β(C11–H21)	1151	β(C11–H21)	1154	β (C11–H21)
	1127 vw					1128	ν(C–N)dimer
1111 sh						1112	$\beta R_{1\ phenyl\ 1}$
1105 m	1105 w			1093	ν(C5–N4)	1092	ν (C33–Cl48) $\beta R_{1\ phenyl\ 2}$
1091 w	1091 s	1083	ν(C8–Cl23)	1079	$\beta R_{1\ phenyl}$	1082	δ(N4H18Cl25)
1075 w	1071 m	1074	ν(C5–N4)	1066	ν(C10–C11)	1079	$\beta R_{1\ phenyl\ 2}$ ν (C30–N29)
1069 w		1064	ν(C10–C11)	1033	ν(C1–N2)	1070	ν (C5–N4)
1026 w	1028 m	1026	τw CH_2 (C5)	1023	τw CH_2 (C5)	1023	τw CH_2 (C5)
	1014 m	1016	ν(C1–N2)	994	ν(C5–N4)	1010	ν (C1–N2)
	987 vw	986	ν (C3–N2)			995	τw CH_2 (C30) τw CH_2 (C26)
973 w	973 vw	969	γ (C11–H21)	951	γC11-H21	964	γ(C36–H46)
928 w	929 s	929	δ (N4H18Cl25)			922	γ(C12–H20)
	898v w	901	ν(C1–C5)	908	ν(C1–C5)	903	ν (C30–C26)
	877 vw	892	γ C10–H20	876	γ C12–H22	871	δ(N29H43Cl50)
862 w	863 m	859	$\beta R_{1\ phenyl}$	867	$\beta R_{1\ phenyl}$ $\beta R_{2\ imid}$	857	$\beta R_{2\ imid.2}$
	840 vw			846	$\beta R_{2\ imid}$	854	$\beta R_{1\ phenyl\ 1}$
	828 vw					832	τ(N4H18Cl25H49)
812 sh		809	τw CH_2 (C1)	806	τ (.Cl25–H18–N4–C)	811	γ(C10–H22)
795 m	794 w	797	$\beta R_{1\ imid.}$	802	$\tau R_{1\ phenyl}$	802	τ(Cl25H18N4C)[c]
778 s	778 vw	773	γ (C12–H22)	767	$\beta R_{2\ phenyl}$	774	γ(C37–H47)

Table 2 (*continued*)

Experimental[a]		Hydrochloride[a]		Anionic Form[a]		Dimer[a]	
IR	Raman	SQM[b]	Assignment[a]	SQM[b]	Assignment[a]	SQM[b]	Assignment[a]
	766 w	758	$\beta R_{2\ phenyl}$	765	γ C10–H20	757	ν (C34–Cl44
	747 vw			752	γ N2–H17	752	$\beta R_{2\ phenyl.1}$
	713 vw	706	$\tau R_{1\ phenyl}$; $\tau R_{2\ imid}$	705	γ C3–N6	711	$\beta R_{2\ imid.1}$
694 m	696 w, br			673	$\beta R_{1\ imid}$	703	$\tau R_{1\ phenyl\ 2}$
686 m		680	$\beta R_{2\ imid.}$	671	τ (Cl26–H24–N6–C)	681	$\tau R_{1\ phenyl\ 1}$
669 w		670	γ (C3–N6)	665	τw CH_2 (C1)	676	γ(C3–N6)
638 w	645 m	640	$\tau R_{1\ phenyl}$	636	$\beta R_{3\ phenyl}$	635	τ(N31H49Cl25H18)
618 sh	600 vw					608	γ(N31–H49)
	587 vw					536	β (C32–N31)
	578 vw	545	β(C7–N6)	536	β(C7–N6)	533	β (C7–N6)
532 w	537 w	532	γ (N2–H17)			525	γ (N2–H17
525 w	522 w					521	γ (C8–Cl19)
							γ (C9–Cl23)
518 w		513	γ (C8–Cl23)	518	γ C8–Cl23		
501 w	505 m			501	$\tau R_{3\ phenyl}$	495	γ (C32–N31)
					γ C7–N6		
486 w		490	$\tau R_{3\ phenyl}$			490	$\tau R_{3\ phenyl\ 1}$
462 vw	443 s					440	δ (C–N–C)[c]
437 vw	437 sh	435	γ (N6–H24)			427	β (C28–N31)
421 w, br				430	ν (C8–Cl23)	424	ν (C9–Cl23)
406 w	408 vs	407	β (C3–N6)			402	$\beta R_{2\ phenyl\ 2}$
402 vw		396	ν (C9–Cl19)	401	ν (C9–Cl19)	399	ν (C8–Cl19)
						388	γ(N6–H24)
	326 m	323	$\beta R_{3\ phenyl}$	324	β (C3–N6)	334	$\tau R_{2\ imid.2}$
	303 sh	299	$\tau R_{2\ imid.}$	301	β (C9–Cl19)	318	$\beta R_{3\ phenyl\ 1}$
	293 m					291	$\tau w_{\ imid1.}$
	268 vw	286	γ (C9–Cl19)	287	γ C9–Cl19	284	γ (C7–N6)
	260 vw	238	ν (Cl25–H18)			230	ν (Cl50–H43)
	220 s					204	$\tau R_{2\ phenyl.1}$
	210 sh			208	$\tau R_{1\ imid}$	200	$\tau R_{2\ phenyl\ 2}$
					β(C9–Cl19)		$\tau R_{3\ phenyl\ 2}$
		200	$\tau R_{2\ phenyl}$	202	$\tau R_{1\ imid}$	199	β (C9–Cl23)
							β (C8–Cl19)
		195	β (C8–Cl23)	196	$\tau R_{2\ phenyl}$	192	γ(N4–H18)
	186 vw			185	β (C8–Cl23)		
		176	β (C9–Cl19)			178	$\tau R_{2\ imid1.}$
	169 w, br			166	$\tau R_{2\ imid}$	162	γ (N27–H42)
	126 vw	147	$\tau R_{1\ imid.}$	154	ν (Cl25–H18)	149	$\tau R_{1\ imid.2}$
	119 vw	113	γ (C7–N6)			125	ν (Cl25–H18)
	109 vw			111	δ (C3–N6–C7)	116	δ (N4–H18–Cl25)[c]
		67	τ(.Cl25H18N4C)	92	$\tau w_{\ imid.}$	105	γ(N29–H43)
				78	ν (Cl26–H24)		
		63	δ (C3–N6–C7)	56	δ (N6–H24–Cl26)	57	δ(Cl25–H49–N31)
		56	$\tau w_{\ imid}$			53	$\tau w_{\ imid.2}$
				45	δ (N4–H18–Cl25)		
		32	$\tau w_{\ phenyl.}$	35	γN6-H24	35	$\tau w_{\ phenyl\ 1}$
		20	γ (N4–H18)	21	γN4-H18		
				18	$\tau w_{\ phenyl}$		

Abbreviations: ν, stretching; β, deformation in the plane; γ, deformation out of plane; wag, wagging; τ, torsion; β_R, deformation ring; τ_R, torsion ring; ρ, rocking; τw, twisting; δ, deformation; a, antisymmetric; s, symmetric; imid., imidazoline ring.

[a] This work.

[b] From scaled quantum mechanics force field.

[c] Assigned using the Gauss View program [18].

863 cm^{-1}. Moreover, the torsion rings modes for the phenyl ring were assigned to IR bands at 694 and 486 cm^{-1} for imidazole these bands appear in the Raman spectrum at 326 and 126 cm^{-1}.

5. Force field

The Molvib program [20] was used to calculate the force constants of clonidine hydrochloride, expressed in terms of internal coordinates, from the corresponding scaled force fields. These constants were calculated in the gas phase at the B3LYP/6-31G* and B3LYP/6-311++G** levels and, then, they were compared in Table 3 with those obtained for 2-(-2-benzofuranyl)-2-imidazoline [7] and for the protoned species of tolazoline hydrochloride [8] by using both methods. Here, it is notable the influence of the size of the basis sets on the calculated force constants values, as observed in Table 3. Thus, the values increase when the size of the basis set change of 6–31G* at 6-311++G**. The results show that the presence of the Cl atoms in the benzyl rings increase the $f(\nu N{-}C)$ and $f(\nu C{-}H)_{benc}$ force constants, in relation to the two species compared. On the other hand, the $f(\nu C{-}C)_{imid}$ and $f(\nu C{-}H)_{imid}$ force constants of tolazoline hydrochloride [8] present the highest value in relation to clonidine hydrochloride indicating, this way, that the imidazoline rings are also influenced by the Cl atoms of the benzyl rings. Another important observation, is that the presence of Cl atoms in the hydrochloride form increase the $f(\nu C{-}Cl)$ and $f(\nu C{-}C)_{benc}$ force constants values while decrease the $f(\nu N{-}H)$ force constant value, as expected because the N–H bond are linked to that H → Cl bond. This latter result could explain the high reactivity

Table 3
Comparison of scaled internal force constants for clonidine hydrochloride using two levels of theory.

Description	B3LYP[a]							
	6-31G*				6-311++G**			
	H	A	BFI[b]	T[c]	H	A	BFI[b]	T[c]
f(νN-H)	5.21	4.89	6.53	6.68	5.33	4.99	6.57	6.66
f(νN-C)	6.11	6.32	4.75	4.48	5.99	6.17	4.63	4.38
$f(\nu C\text{-}H)_{imid}$	4.67	4.59	4.78	4.94	4.60	4.53	4.72	4.86
$f(\nu C\text{-}H)_{benc}$	5.26	5.23	5.17	5.17	5.18	5.16	5.10	5.09
f(νC-Cl)	3.32	3.35			3.28	3.30		
f(νCl-H)	0.88	0.43			0.81	0.39		
$f(\nu C\text{-}C)_{imid}$	3.94	3.93	3.86	4.21	3.89	3.88	3.81	4.12
$f(\nu C\text{-}C)_{benc}$	6.58	6.52	6.58	6.50	6.46	6.41	6.50	6.02
$f(\beta_{R\ benc})$	0.22	0.22	0.35	0.22	0.22	0.22	0.35	0.22
$f(\beta_{R\ imid})$	0.33	0.34		0.34	0.33	0.34		0.34
$f(\gamma\ C\text{-}H)$	0.44	0.42		0.47	0.43	0.42		0.47

Units in mdyn $Å^{-1}$ for stretching and mdyn Å rad $^{-2}$ for angle deformations.
ν, stretching; β, deformation; γ, out plane deformation; benc., bencene; imid., imidazoline; R, ring.
[a] This work.
[b] From Ref [7] for 2-(-2-benzofuranyl)-2-imidazoline.
[c] From Ref [8] for the protoned species of tolazoline hydrochloride.

of clonidine hydrochloride in relation to others antihypertensive agents, as will see to continuation.

6. HOMO-LUMO

The reactivity of clonidine hydrochloride was studied by using the frontier orbitals and the values are compared in Table S7 with values calculated in this work for the protonated and hydrochloride species of tolazoline. The results show that both frontier orbitals are mainly located in the rings, suggesting that are antibonding orbital π-type. In the gas phase, clonidine hydrochloride exhibits greater reactivity with both basis sets than the other species compared, as expected because the Cl25 atoms have the highest NPA charge values and, as also was observed in the tolazoline hydrochloride.

7. Conclusions

In the present work, the clonidine hydrochloride was characterized by using the FT-IR and FT-Raman spectra in the solid state. The theoretical molecular structures of the monomeric and dimeric structures of clonidine hydrochloride were determined by the B3LYP/6-31G* and B3LYP/6-311++G** methods and the calculations suggest the existence of these structures in the gas phase, as were experimentally observed in the packing crystalline of the solid. The assignments of the all normal modes of vibration for clonidine hydrochloride and their dimer are reported at the B3LYP/6-31G* level of theory. The complete force fields have been determined, as well as the principal force constants for stretching and deformation modes for both species. The NBO and AIM studies evidence the covalent and ionic characteristics of the N4—H18 and H18→Cl25 bonds, respectively. The high reactivity of clonidine hydrochloride could be explained by the ionic nature of the H18→Cl25 bond and by the high values of the *LP(1)N4 → LP*(1) H18* charge transfers that evidently stabilize the system during the reaction.

Acknowledgements

This work was subsidized with grants from CIUNT Project No 26/D507 (Consejo de Investigaciones, Universidad Nacional de Tucumán). The authors thank Prof. Tom Sundius for his permission to use Molvib.

Appendix A. Supplementary data

Supplementary data related to this article can be found at http://dx.doi.org/10.1016/j.molstruc.2016.12.008.

References

[1] R.R. Ruffolo Jr., W. Bondinell, J.P. Hieble, α- and β-Adrenoceptors: from the gene to the clinic. 2. Structure-activity relationships and therapeutic applications, J. Med. Chem. 38 (19) (1995) 3681–3716.
[2] M. Remko, O.A. Walsh, W.G. Richards, Molecular structure and gas-phase reactivity of clonidine and rilmenidine: two-layered ONIOM calculations, Phys. Chem. Chem. Phys. 3 (2001) 901–907.
[3] C. Farsang, J. Kapocsi, Imidazoline receptors: from discovery to antihypertensive therapy (facts and doubts), Brain Res. Bull. 49 (5) (1999) 317–331.
[4] M. Remko, M. Swart, F.M. Bickelhaup, Theoretical study of structure, pKa, lipophilicity, solubility, absorption, and polar surfaces area of some centrally acting antihypertensives, Bioorg. Med. Chem. 14 (2006) 1715–1728.
[5] B. Baranowska, J. Tremblay, J. Gutkowska, Clonidine stimulates atrial natriuretic factor (ANF) release in water-deprived rats, Peptides 9 (1988) 189–192.
[6] J. Tank, A. Diedrich, E. Szczech, F.C. Luft, J. Jordan, α-2 adrenergic transmission and human baroreflex regulation, Hypertension 43 (2004) 1035–1041.
[7] C.D. Contreras, M. Montejo, J.J. López González, J. Zinczuk, S.A. Brandán, Structural and vibrational analyses of 2-(2-benzofuranyl)-2-imidazoline, Raman Spect. 42 (1) (2011) 108–116.
[8] C.D. Contreras, A.E. Ledesma, J. Zinczuk, S.A. Brandán, Vibrational study of tolazoline hydrochloride by using FTIR-raman and DFT calculations, Spectrochim. Acta Part A 79 (2011) 1710–1714.
[9] a) G. Rauhut, P. Pulay, J. Phys. Chem. 99 (1995) 3093–3099;
b) Correction G. Rauhut, P. Pulay, J. Phys. Chem. 99 (1995) 14572.
[10] A.E. Reed, L.A. Curtis, F. Weinhold, Intermolecular interactions from a natural bond orbital, donor-acceptor viewpoint, Chem. Rev. 88 (6) (1988) 899–926.
[11] E.D. Glendening, J.K. Badenhoop, A.D. Reed, J.E. Carpenter, F. Weinhold, NBO 3.1, Theoretical Chemistry Institute, University of Wisconsin, Madison, WI, 1996.
[12] R.F.W. Bader, Atoms in Molecules, a Quantum Theory, Oxford University Press, Oxford, 1990, ISBN 0198558651.
[13] F. Biegler-Köning, J. Schönbohm, D. Bayles, AIM2000; a program to analyze and visualize atoms in molecules, J. Comput. Chem. 22 (2001) 545.
[14] A.B. Nielsen, A.J. Holder, Gauss View 3.0, User's Reference, GAUSSIAN Inc., Pittsburgh, PA, 2000–2003.
[15] A.D. Becke, Density-functional exchange-energy approximation with correct asymptotic behavior, Phys. Rev. A38 (1988) 3098–3100.
[16] C. Lee, W. Yang, R.G. Parr, Development of the Colle-Salvetti correlation-energy formula into a functional of the electron density, Phys. Rev. B 37 (1988) 785–789.
[17] M.J. Frisch, G.W. Trucks, H.B. Schlegel, G.E. Scuseria, M.A. Robb, J.R. Cheeseman, J.A. Montgomery Jr., T. Vreven, K.N. Kudin, J.C. Burant, J.M. Millam, S.S. Iyengar, J. Tomasi, V. Barone, B. Mennucci, M. Cossi, G. Scalmani, N. Rega, G.A. Petersson, H. Nakatsuji, M. Hada, M. Ehara, K. Toyota, R. Fukuda, J. Hasegawa, M. Ishida, T. Nakajima, Y. Honda, O. Kitao, H. Nakai, M. Klene, X. Li, J.E. Knox, H.P. Hratchian, J.B. Cross, C. Adamo, J. Jaramillo, R. Gomperts, R.E. Stratmann, O. Yazyev, A.J. Austin, R. Cammi, C. Pomelli, J.W. Ochterski, P.Y. Ayala, K. Morokuma, G.A. Voth, P. Salvador, J.J. Dannenberg, V.G. Zakrzewski, S. Dapprich, A.D. Daniels, M.C. Strain, O. Farkas, D.K. Malick, A.D. Rabuck, K. Raghavachari, J.B. Foresman, J.V. Ortiz, Q. Cui, A.G. Baboul, S. Clifford, J. Cioslowski, B.B. Stefanov, G. Liu, A. Liashenko, P. Piskorz, I. Komaromi, R.L. Martin, D.J. Fox, T. Keith, M.A. Al-Laham, C.Y. Peng, A. Nanayakkara, M. Challacombe, P.M.W. Gill, B. Johnson, W. Chen, M.W. Wong, C. Gonzalez, J.A. Pople, Gaussian 03, Revision B.01, Gaussian, Inc., Pittsburgh PA, 2003.
[18] S.F. Boys, F. Bernardi, The calculation of small molecular interactions by the differences of separate total energies. Some procedures with reduced errors, Mol. Phys. 19 (1973) 553.
[19] T. Sundius, Scaling of ab initio force fields by MOLVIB, Vib. Spectrosc. 29 (2002) 89–95.
[20] P.L. Polavarapu, Ab initio vibrational Raman and Raman optical activity spectra, J. Phys. Chem. 94 (1990) 8106.
[21] G. Keresztury, S. Holly, G. Besenyei, J. Varga, A.Y. Wang, J.R. Durig, Spectrochim. Acta 49A (1993) 2007–2026.
[22] D. Michalska, R. Wysokinski, Chem. Phys. Lett. 403 (2005) 211–217.
[23] E. Romano, A.B. Raschi, A.M. Benavente, S.A. Brandán, Structural analysis, vibracional spectra and coordinated normal of 2R-(_)-6-hydroxytremetone, Spectrochim. Acta Part A Mol. Biomol. Spectrosc. 84 (2011) 111–116.
[24] E. Romano, M.V. Castillo, J. Pergomet, J. Zinczuk, S.A. Brandán, Synthesis, structural study and spectroscopic characterization of a quinolin-8-yloxy derivative with potential biological properties, Open J. Synthesis Theory Appl. 2 (2013) 8–22.
[25] E. Romano, F. Ladetto, S.A. Brandán, Structural and vibrational studies of the potential anticancer agent, 5-difluoromethyl-1,3,4-thiadiazole-2-amino by DFT calculations, Comput. Theor. Chem. 1011 (2013) 57–64.
[26] E. Romano, S.A. Brandán, Vibrational analysis of the tautomers of the α-adrenergic agonist clonidine agent and their protonated species, ChemXpress

9 (2) (2016) 192–205.
[27] G. Byre, A. Mostad, C. Roming, Crystal and molecular structure of clonidine hydrochloride, 2-(2,6-Dichlorophenylamino)-2-imidazoline hydrochloride, Acta Chem. Scand. B 30 (1976) 843–846.
[28] S. Ghose, J.K. Dattagupta, Crystal structure of tolazoline hydrochloride (priscoline), an α-adrenergic antagonist, J. Chem. Soc. Perkin Trans. II (1989) 599–601.
[29] D. Romani, S.A. Brandán, Structural and spectroscopic studies of two 1,3-benzothiazole tautomers with potential antimicrobial activity in different media. Prediction of their reactivities, Comput. Theor. Chem. 1061 (2015) 89–99.
[30] D. Romani, M.J. Márquez, M.B. Márquez, S.A. Brandán, Structural, topological and vibrational properties of an isothiazole derivatives series with antiviral activities, J. Mol. Struct. 1100 (2015) 279–289.